The Journal of Chemical Physics ARTICLE scitation.org/journal/jcp

Diarsine- vs diphosphine-protected Au_{13} clusters: Effect of subtle geometric differences on optical property and electronic structure

Cite as: J. Chem. Phys. 155, 054301 (2021); doi: 10.1063/5.0059607
Submitted: 10 June 2021 • Accepted: 18 July 2021 •
Published Online: 2 August 2021

Yukatsu Shichibu,[1,2,a] Fan Zhang,[1] Yuxiang Chen,[1] Masafumi Konishi,[3] Susumu Tanaka,[3] Hiroaki Imoto,[3] Kensuke Naka,[3] and Katsuaki Konishi[1,2,a]

AFFILIATIONS

[1] Graduate School of Environmental Science, Hokkaido University, North 10 West 5, Sapporo 060-0810, Japan
[2] Faculty of Environmental Earth Science, Hokkaido University, North 10 West 5, Sapporo 060-0810, Japan
[3] Faculty of Molecular Chemistry and Engineering, Graduate School of Science and Technology, Kyoto Institute of Technology, Goshokaido-cho, Matsugasaki, Sakyo-ku, Kyoto 606-8585, Japan

Note: This paper is part of the JCP Special Topic on From Atom-Precise Nanoclusters to Superatom Materials.
[a] **Authors to whom correspondence should be addressed:** shichibu@ees.hokudai.ac.jp and konishi@ees.hokudai.ac.jp

ABSTRACT

In the design of ligand-protected metal clusters, the choice of protecting ligands is a critical factor because they can profoundly affect the nuclearity, geometry, and electronic structures to afford a diverse range of cluster compounds. Here, we report the synthesis of two novel diarsine-protected Au_{13} clusters ($[Au_{13}L_5Cl_2]^{3+}$, L = diarsine) and compare these clusters with diphosphine analogs in terms of the core geometry and optical properties. In the crystal structure, the cluster bearing C3-bridged diarsines {$[Au_{13}(dpap)_5Cl_2]^{3+}$, **3**} had an apparently identical icosahedral Au_{13} core to $[Au_{13}(dppe)_5Cl_2]^{3+}$ (**1**) with C2-bridged diphosphines, but slight structural differences associated with the bridging unit of the ligands were found. Despite similar icosahedral Au_{13} cores **1** and **3**, their absorption and photoluminescence profiles were evidently different. Theoretical calculations revealed that the subtle deformation of the Au_{13} icosahedron, rather than the coordinating atoms (As or P), notably influences the electronic structure to cause the difference in the absorption profiles.

I. INTRODUCTION

Ligand-protected gold clusters have attracted growing attention recently because of their unique physicochemical properties that can be tuned by the core nuclearity, geometry, and shape as well as the protecting ligands.[1,2] Among various core geometries of gold clusters, icosahedral Au_{13}, which is ubiquitously found in numerous ligand-protected gold clusters, has been greatly highlighted.[3–14] We have previously established a facile HCl-promoted route that selectively affords diphosphine-protected Au_{13} clusters {i.e., $[Au_{13}L_5Cl_2]^{3+}$ for n = 2 and $[Au_{13}L_4Cl_4]^{+}$ for n = 3–5; L = $Ph_2P(CH_2)_nPPh_2$}.[6,15] This method opened the door to various M_{13} clusters, promoting the syntheses of a series of related Au_{13} clusters protected by various neutral (e.g., stibine[16] and N-heterocyclic carbene[17]) and anionic (e.g., acetylide[18] and halide[19]) ligands to elicit unique aspects of Au_{13} clusters (i.e., NIR emission,[6,15,17] $^1O_2$ generation,[20] and chiroptical activity[21,22]).

Arsines have widely been used as alternative ligands to phosphines for various metal complexes because of similar chemical properties of phosphorus and arsenic.[23–25] However, they have been rarely used for the protection of gold clusters,[26,27] and no examples of diarsine-protected gold clusters have been reported. In this paper, we report the synthesis, characterization, single-crystal x-ray diffraction structure, and optical properties of novel diarsine-protected $[Au_{13}L_5Cl_2]^{3+}$-type clusters and discuss the effects of arsenic ligands on the geometric and electronic structures in comparison with the phosphino analogs. We show that the swapping of diphosphine to diarsine results in the formation of Au_{13} species with different compositions and/or absorption spectral patterns. Experimental data together with theoretical investigation based on the crystal structures showed that a subtle difference in the icosahedral core structures causes a significant perturbation on the optical properties and electronic structures.

II. EXPERIMENTAL AND THEORETICAL METHODS

A. Materials

Acetonitrile (99%), dichloromethane (99%), and toluene (99%) were purchased from Kanto Chemical Co., Inc. Ethanol (99%), benzene (99%), and hydrochloric acid (35%–37%) were obtained from Fujifilm Wako Pure Chemical Corporation. Sodium borohydride (>95%) was obtained from TCI Co., Ltd. Sodium hexafluoroantimonate (99%) was obtained from Sigma-Aldrich. All reagents were used as received. Diarsine ligands, dpae [1,2-bis(diphenylarsino)ethane] and dpap [1,3-bis(diphenylarsino)propane], were synthesized following the literature procedures.[28,29] The precursors $Au_2(dpae)Cl_2$ and $Au_2(dpap)Cl_2$ were prepared from $AuCl(SMe_2)$ and the corresponding diarsines according to the literature with some modifications.[15,30]

B. Syntheses of the Au_{13} clusters

$[Au_{13}(dpae)_5Cl_2]Cl_3$ ($\mathbf{2}\cdot Cl_3$) was obtained from the reduction in the gold–diarsine complex followed by HCl treatment.[6] To an ice-cooled dichloromethane solution (32 ml) of $Au_2(dpae)Cl_2$ (121.8 mg, 128.1 μmol) was added an ethanol solution (1.5 ml) of sodium borohydride (4.8 mg, 130 μmol), and the mixture was stirred for 1 h at 0 °C and 2 h at 25 °C. Subsequently, the resulting dark red solution was treated with 12M HCl (107 μl, 1.284 mmol) and stirred for two days. After removal of precipitates by filtration, the filtrate was evaporated, washed with benzene, and redissolved in ethanol. The ethanolic solution after filtration was evaporated to dryness to give $\mathbf{2}\cdot Cl_3$ as a brown solid (37.4 mg; 37% based on Au). $[Au_{13}(dpap)_5Cl_2]Cl_3$ ($\mathbf{3}\cdot Cl_3$) was obtained in a similar manner to the synthesis of $\mathbf{2}\cdot Cl_3$. To an ice-cooled dichloromethane solution (26 ml) of $Au_2(dpap)Cl_2$ (100 mg, 104 μmol) was added an ethanolic solution (1 ml) of sodium borohydride (3.9 mg, 100 μmol), and the mixture was stirred for 1 h at 0 °C and 2 h at 25 °C. The resulting brownish solution was mixed with 12M HCl (86 μl, 1.032 mmol), and the mixture was stirred for 26 h. After the same purification process of $\mathbf{2}\cdot Cl_3$, an orange solid of $\mathbf{3}\cdot Cl_3$ was obtained (34.7 mg; 42% based on Au). $[Au_{13}(dpap)_5Cl_2](SbF_6)_3$ [$\mathbf{3}\cdot(SbF_6)_3$] was obtained by the anion exchange reaction of $\mathbf{3}\cdot Cl_3$ with excess $NaSbF_6$ in ethanol. Crystal of $\mathbf{3}\cdot(SbF_6)_3$ suitable for x-ray analysis was grown from toluene/dichloromethane (1:1).

C. Measurements

Electrospray ionization (ESI) mass spectrometry was performed using a Bruker micrOTOF-HS mass spectrometer. Optical absorption and photoluminescence spectra were recorded using JASCO V-670 and FP-8600 spectrometers, respectively. Photoluminescence quantum yields were determined relative to rhodamine 6 G in ethanol. Crystal data were collected on a Rigaku XtaLAB Synergy DW diffractometer with graphite-monochromated Cu K_α radiation (λ = 1.541 84 Å). The crystal structure was solved by direct methods and expanded using Fourier techniques. All non-hydrogen atoms were refined using the riding model. All calculations were performed using the Olex2 crystallographic software package except for refinement, which was performed using SHELXL-2018.[31]

D. Computational details

All calculations were performed using density functional theory (DFT) or time-dependent DFT (TDDFT) methods with a TURBOMOLE package.[32] Crystallographically determined structures of the clusters (**1** and **3**) were adopted as the initial geometries for the geometry-optimization calculations, which were computed at the BP86/double-ζ plus polarization (def-SVP) level.[33] Single-point and absorption-spectrum calculations were performed at the B3LYP level[34,35] with basis sets of triple-ζ valence plus polarization quality (def2-TZVP for Au) and split valence plus polarization quality (def2-SVP for the other elements).[36] In all calculations, the default 60-electron relativistic effective core potential (ECP)[37] was employed for the Au atoms, and the resolution of identity (RI) approximation for Coulomb interactions[38] was used for speeding up. The Au_{13}-core-fixed arsenic counterpart of **1** was built from the geometry-optimized **1**, followed by a replacement of the coordinating atoms (i.e., P with As) and a re-optimization of only the ligands' structures. The Au_{13}-core-fixed phosphorus counterpart of **3** was built similarly.

III. RESULTS AND DISCUSSION

A. Synthesis and characterization of diarsine-protected Au_{13} clusters

The syntheses of Au_{13} clusters protected by diarsine ligands with C2 and C3 alkyl bridges (dpae and dpap, respectively) were examined using the established two-step method involving the HCl-induced nuclearity convergence.[6,15] Our previous reports showed that the use of the C2-bridged diphenylphosphino ligands (dppe) results in the selective formation of trivalent $[Au_{13}L_5Cl_2]^{3+}$ (Scheme 1), whereas monovalent $[Au_{13}L_4Cl_4]^+$ is obtained with the C3-bridged diphenylphosphino ligands (dppp). Unlike them, dpae and dpap both afforded $[Au_{13}L_5Cl_2]^{3+}$-type clusters (**2** and **3,** respectively) (Scheme 1). For instance, the Au_{13} clusters, which was isolated from the reaction mixtures as sole cluster products, both showed signals assignable to $[Au_{13}L_5Cl_2]^{3+}$ in the ESI mass spectra (Fig. 1). No other signals, such as those of $[Au_{13}L_4Cl_4]^+$, which should appear around m/z = ~5000, were observed. The different behaviors of the C3-bridged ligands (dppp vs dpap) suggest that the subtle difference in the ligating atoms, e.g., size and donating capability, can affect the ligation patterns as well as the geometric and electronic structures of the Au_{13} clusters.

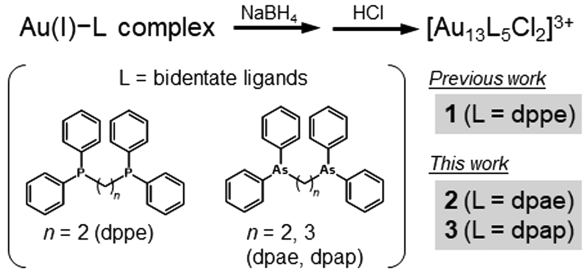

SCHEME 1. Two-step synthesis of $[Au_{13}L_5Cl_2]^{3+}$ clusters (top). The bidentate ligands used in the previous (bottom left) and this (bottom middle) works.

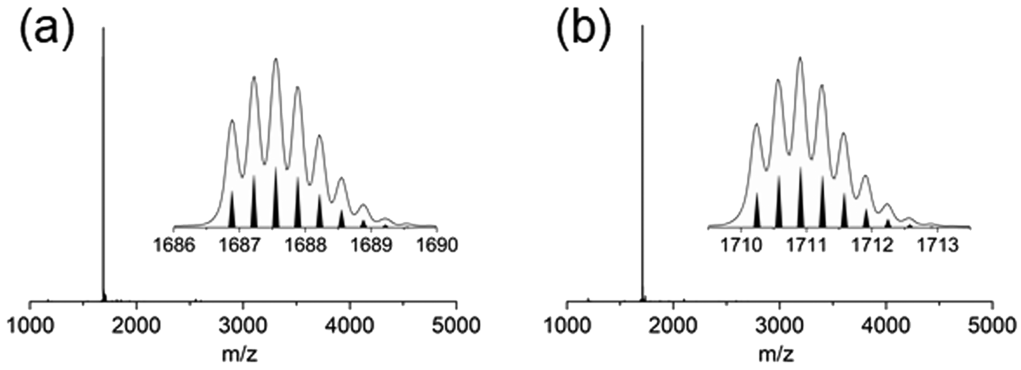

FIG. 1. ESI mass spectra of (a) **2** and (b) **3**. The insets show the comparison between experimental data and calculated isotope patterns.

B. Geometric features

Single-crystal x-ray diffraction analysis was successful for **3**, and the structure of one of the cluster moieties is shown in Fig. 2. As was the case with the diphosphine-type $[Au_{13}L_5Cl_2]^{3+}$, clusters such as **1**, **3** contained an icosahedral Au_{13} core protected by two anionic ligands at the *trans*-positions and five chelating ligands at the quasi-equatorial direction [Fig. 2(a)]. As shown in Fig. 2(b), two Au_5 rings sandwich a central Au atom with a staggered conformation to form a tube-shaped Au_{10} moiety cross-linked by five diarsine ligands. In a previous paper, we showed the chirality of diphosphine-protected Au_{13} clusters depending on the handedness of the cross-linkage arrangements.[22] Likewise, the helical crosslinking arrangements of the diarsine ligands result in the emergence of chirality, namely, *P*- (Fig. 2) and *M*-helicity. In the crystal structure of **3**, equal amounts of the enantiomers were found, indicating that the crystal was obtained as a racemic compound (Fig. S1 and Table S1).

Table I summarizes the selected structural parameters of **1** and **3**. The difference in the average distances of all Au–Au bonds between **1** (2.865 Å) and **3** (2.862 Å) was negligibly small (i.e., 0.003 Å), but the detailed comparison revealed definite differences. In the Au_{10} tube composed of the two Au_5 pentagons [Fig. 2(b)], the Au–Au bonds of **3** related to the cross-linked diarsines (d_1) tended to be longer than the adjacent distances (d_2) (Fig. S2), where the average distance of d_1 (2.921 Å) was longer by 0.035 Å than that of d_2 (2.886 Å) (Table I). In addition, the dihedral angles of **3** relating to the cross-linked diarsines (θ_1) were mostly wider than the adjacent angles (θ_2) (Fig. S2), and their average angles from the ideal staggered angle of 36° (i.e., $\theta_1 - 36$ and $\theta_2 - 36$) were +0.80° and −0.80°, respectively (Table I). These trends associated with the cross-linked (d_1, θ_1) and uncross-linked (d_2, θ_2) Au atoms are opposite to those of the known Au_{13} cluster (**1**) protected by C2-bridged diphosphines.[22] The average distances between the coordinating atoms of each bidentate ligand for **1** and **3** (i.e., P–P and As–As distances) were 4.085 and 4.950 Å, respectively. This difference can be correlated with larger d_1 and θ_1 for **3** than for **1**, indicating the effect of the ligand-induced strains on the Au_{13} cores. Considering that arsenic atom would allow less rigid bridging environment because of the larger size, the difference in the orientation of the two pentagons of **1** and **3** may reflect the degree of the steric restriction of the bridging methylene chains.

It should be also noted that the longer C3 bridge of the dpap ligand induces substantial deformation of the icosahedral core of **3**. For instance, the distance between the two axial Cl-coordinated gold atoms [z_1 in Fig. 2(a) and Table I] for **3** was 5.426 Å, which is 0.033 Å longer than that for **1** (5.393 Å). On the contrary, the Au–Au bonds between the central Au atom and the peripheral As-coordinated Au atoms [r_1 in Fig. 2(a) and Table I] for **3** gave a slightly shorter length in average (2.769 Å) than the corresponding bonds in **1** (2.777 Å). Thus, the Au_{13} core slightly shrinks laterally and expands along the Cl-containing longitudinal axis [i.e., the z axis in Fig. 2(a)] when the C2-bridged diphosphine (dppe) ligands of **1** are swapped to the C3-bridged diarsine (dpap) ligands (**3**). Accordingly, for the Au–Au bonds connecting the two Au_5 pentagons (d_1 and d_2), **3** gave a longer average length than **1** (2.904 Å vs 2.886 Å), while the average distance of the Au–Au bonds comprising the Au_5 rings [d_3 in Fig. 2(b) and Table I] for **3** (2.916 Å) was shorter by 0.017 Å than that for **1** (2.933 Å). These observations indicate that the steric restriction

TABLE I. Average distances and angles (d_1, d_2, d_3, z_1, r_1, $\theta_1 - 36$ and $\theta_2 - 36$, Fig. 2) of **1** and **3** (with standard deviations).[a]

	d_1 (Å)	d_2 (Å)	d_3 (Å)	z_1 (Å)	r_1 (Å)	$\theta_1 - 36$ (deg)	$\theta_2 - 36$ (deg)
1	2.863 ± 0.016	2.908 ± 0.017	2.933 ± 0.024	5.393	2.777 ± 0.014	−1.03 ± 0.97	+1.03 ± 0.92
	[2.848, 2.889]	[2.884, 2.929]	[2.894, 2.974]		[2.757, 2.798]	[−2.67, +0.20]	[−0.14, +2.37]
3	2.921 ± 0.027	2.886 ± 0.016	2.916 ± 0.042	5.426	2.769 ± 0.017	+0.80 ± 0.93	−0.80 ± 1.19
	[2.881, 2.950]	[2.864, 2.908]	[2.867, 3.006]		[2.741, 2.797]	[−0.77, +2.11]	[−2.63, +0.91]

[a]The minimum and maximum values are given in square brackets.

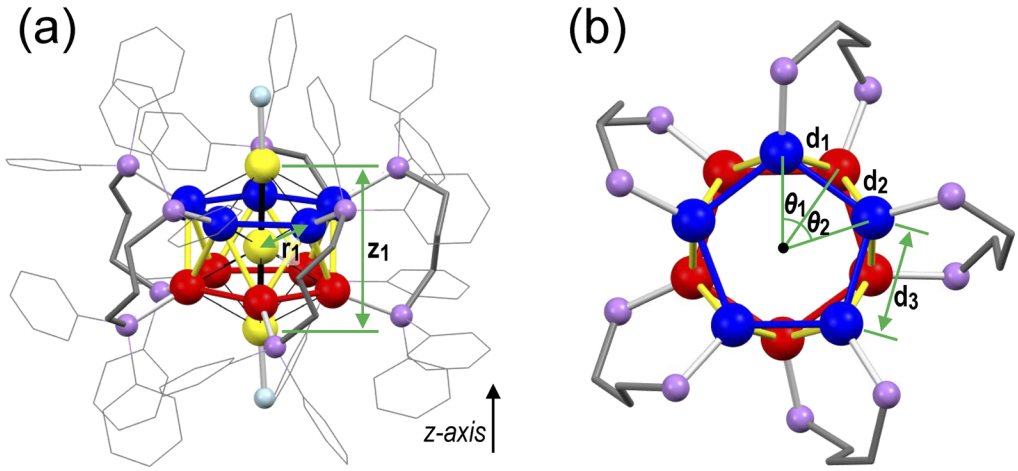

FIG. 2. Geometric structure of (a) **3** (*P*-helicity) and (b) top view of the $Au_{10}L_5$ tube. The dihedral angles (θ_1 and θ_2) are defined between two adjacent planes of Au_3 triangles from two axial chloride-coordinated gold atoms and equatorial arsenic-coordinated gold atoms. The Au–Au bond lengths (d_1 and d_2) are defined between two adjacent gold atoms from the two Au_5 rings. Color codes: yellow/blue/red spheres: Au; purple spheres: As; aqua spheres: Cl; and gray sticks: C. For clarity, the H atoms are omitted.

of the bridging unit of bidentate ligands affects the Au_{13} core structure of $[Au_{13}L_5Cl_2]^{3+}$ clusters. In this regard, it should be interesting to see the structure of the Au_{13} cluster protected by C2-bridged diarsine (dpae) (**2**), but at present, crystals suitable for structural determination were not obtained.

C. Optical properties and electronic structures of Au_{13} clusters

Section III B revealed a slight but definite difference in the Au_{13} core structures between **1** and **3**. To assess the effect of the bidentate ligands on the electronic structures of Au_{13} clusters, we next compared the optical properties of **1** and **3**. The absorption spectrum of **3** showed an intense band at 349 nm and a broadband at 446 nm [Fig. 3(b), blue line], which were fairly blue shifted from the bands

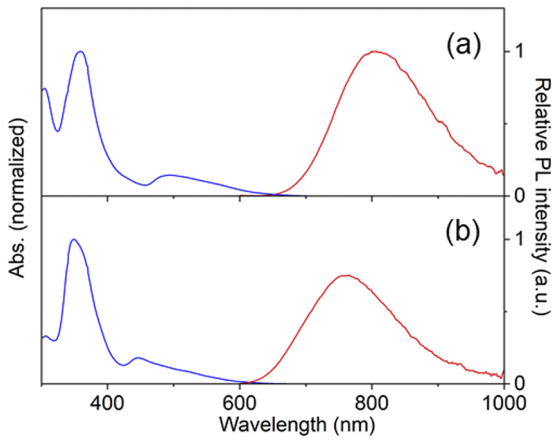

FIG. 3. Absorption (blue line) and photoluminescence (red line) spectra of (a) **1** · $(SbF_6)_3$ (λ_{ex} = 490 nm) and (b) **3** · $(SbF_6)_3$ (λ_{ex} = 445 nm) in MeCN.

of **1** at 360 and 495 nm [Fig. 3(a), blue line]. It should be noted that the spectral profile of **3** was rather similar to that of $[Au_{13}L_4Cl_4]^+$-type clusters bearing C3–C5 bridged diphosphines, which showed an intense asymmetric band at ~340 nm together with a hump at ~430 nm.[15] The photoluminescence properties of **1** and **3** were also compared. **3** displayed an emission peak at 762 nm [Fig. 3(b), red line], which was blue shifted by 43 nm (~0.1 eV) from the peak at 805 nm of **1** [Fig. 3(a), red line]. The quantum yield of **3** was estimated to be 6.9%, which was comparable to that of **1** (8.4%). Thus, the optical properties of **1** and **3** were apparently similar but obviously different, though they both had a similar icosahedral core. On the other hand, the spectral patterns of **2** were evidently dissimilar to those of **1** and **3**. The absorption spectrum was more featureless with a peak at ~340 nm, and the near-IR emission was considerably red-shifted (913 nm) with a quite weak quantum yield (0.1%) (Fig. S3). These spectral features reminded us of those of **1** in dichloromethane[15,20] and suggest that the Au_{13} core can take other isomeric structures, including icosahedron-based variants and non-icosahedral atom packing modes,[39] though a detailed structural study is needed.

The distinctly different optical properties of the geometrically well-defined **1** and **3** were further investigated by means of (TD)DFT theoretical calculations. Geometry optimization calculations of **1** and **3** resulted in essential preservation of the above-mentioned geometric features in the crystal structures (Table S2), so the following calculations were performed with these optimized structures. Figures 4(a) and 4(b) show the molecular orbitals (MOs) of **1** and **3**, which were analyzed in terms of the superatom concept, because the Au_{13} cores can be described as eight-electron superatoms with $1S^21P^61D^0$ configuration. In both **1** and **3**, the MO distribution profiles indicated that HOMO − x ($0 \le x \le 2$) and LUMO + y ($0 \le y \le 4$) were included in the P and D shells, respectively (Figs. S4 and S5). In these MOs, the Au 6s and 5d orbitals contributed dominantly, whereas the contribution of the coordinating atoms (i.e., P or As) was not so significant (<20%) (Tables S3 and S4). The

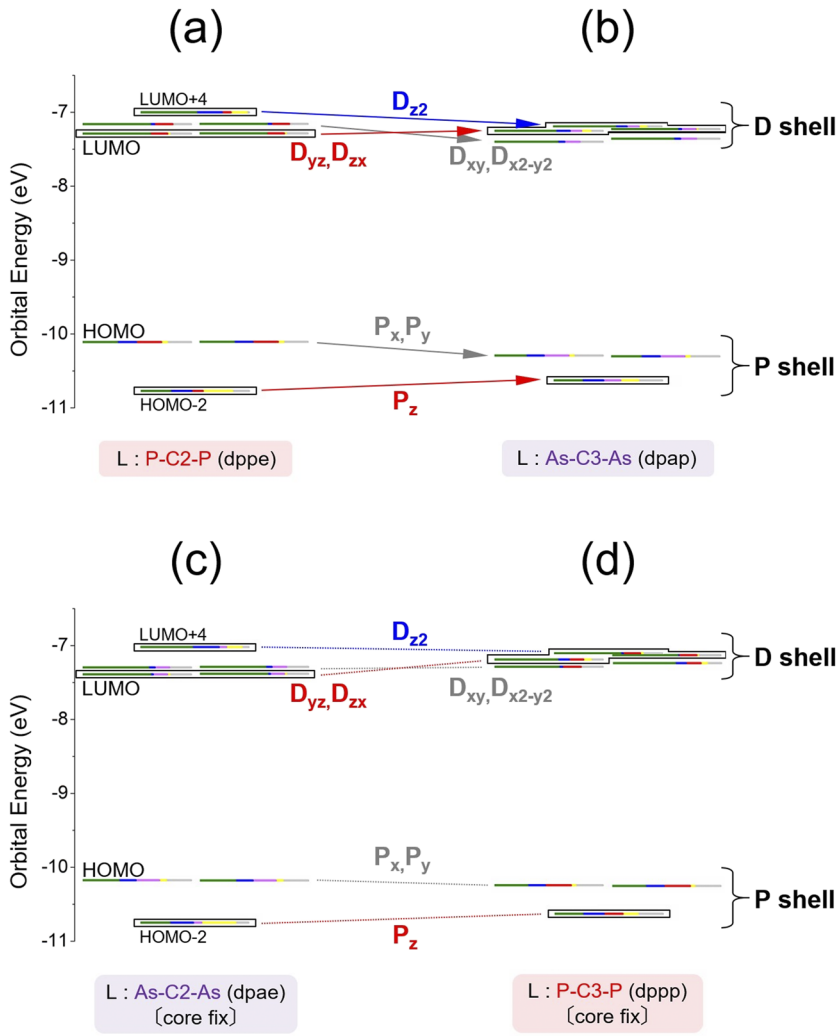

FIG. 4. Kohn–Sham (KS) orbital energy level diagrams of (a) **1**, (b) **3**, (c) the Au_{13}-core-fixed arsenic counterpart of **1**, and (d) the Au_{13}-core-fixed phosphorus counterpart of **3**. Each KS orbital energy is drawn to indicate the relative contributions (line lengths with color labels) of the atomic orbitals of Au (6sp) in green, Au (5d) in blue, P (3p) in red, As (4p) in purple, Cl (3p) in yellow, and others in gray. The MOs with z-components are highlighted in box.

HOMO–LUMO gap energies of **1** (2.82 eV) and **3** (2.89 eV) were quite similar to each other. However, clear differences were especially in the superatomic orbitals involving the z-components (i.e., P_z, D_{yz}, D_{zx}, and D_{z2}) (Fig. 4, highlighted in the box). HOMO − 2 (i.e., P_z) of **3** was more destabilized than that of **1**. On the one hand, regarding the LUMOs, a pair of D_{yz} and D_{zx}, corresponding to LUMO and LUMO + 1 in **1**, was also destabilized and assigned to LUMO + 2 and LUMO + 3 in **3** [Figs. 4(a) and 4(b)]. Moreover, LUMO − 4 (i.e., D_{z2}) of **3** was definitely stabilized, resulting in a very narrow energy gap of 0.06 eV between LUMO + 4 and LUMO + 2 in **3** (Table S4), leading to their hybridization (Fig. S5). It should be interesting to note that similar electronic structure patterns were obtained when the P atoms of **1** and the As atoms of **3** were altered to As and P atoms, respectively, without the relaxation of the original Au_{13} core structures [Figs. 4(c) and 4(d)]. Therefore, the difference in the electronic structure profile of **1** and **3** is not due to the coordinating atoms, rather likely to reflect the subtle deformation of the Au_{13} core along the z axis.

The experimental absorption spectra of **1** and **3** (Fig. 3, blue lines) were theoretically well reproduced. The experimentally observed visible bands [Figs. 5(a) and 5(b), blue dashed lines] likely correspond to the calculated intense bands at 513 and 433 nm for **1** and **3**, respectively [Figs. 5(a) and 5(b)]. These absorptions were mainly attributed to the electronic transitions from the P to D shells within the Au_{13} cores [Figs. 4(a) and 4(b)], for which the MOs with z-components were mostly responsible (Table II, italic letters). Thus, as expected from the electronic structures, the different visible absorption profiles are associated with the deformation of the Au_{13} core mainly along the z-direction. In contrast, the contribution of the coordination atoms (i.e., P and As) to the visible absorptions over 400 nm seemed to be small. In fact, the theoretical absorption spectra of the Au_{13}-core-fixed arsenic counterpart of **1** and phosphorous counterpart of **3** [Figs. 5(c) and 5(d)] were quite similar to those of **1** and **3**, respectively [Figs. 5(a) and 5(b)]. Therefore, the subtle deformation of the icosahedral Au_{13} core was shown to be a main factor to cause a perturbation effect on the experimental absorption profiles.

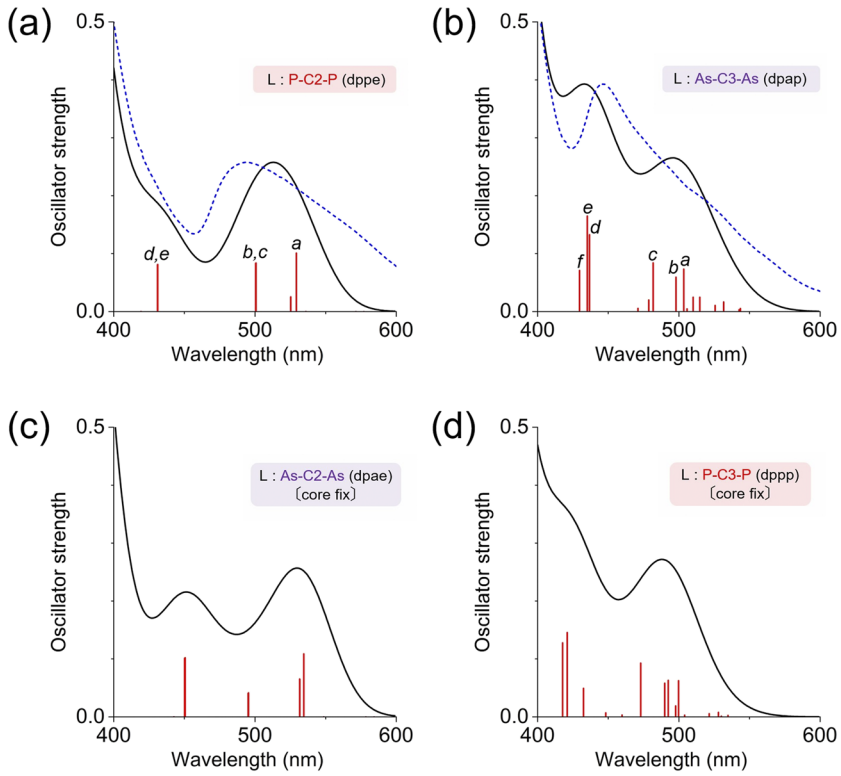

FIG. 5. Theoretical absorption spectra (black solid lines) of (a) **1**, (b) **3**, (c) the Au_{13}-core-fixed arsenic counterpart of **1**, and (d) the Au_{13}-core-fixed phosphorus counterpart of **3**. The heights of the red vertical bars correspond to the calculated oscillator strengths of the individual transitions. Corresponding experimental absorption spectra were given in the blue dashed lines.

TABLE II. Selected excitations of **1** and **3** (with oscillator strength more than 5.0×10^{-2}).

Cluster	Label[a]	Excitation index	Wavelength	Oscillator strength	Dominant contributions[b,c]
1	a	6	529	1.01×10^{-1}	H − 1 → *L*, H → *L* + *1*, H − 1 → *L* + *1*, H → *L*
	b	9	501	8.38×10^{-2}	H → *L* + *4*, H − 1 → L + 3, H → L + 2
	c	10	501	8.33×10^{-2}	H − 1 → *L* + *4*, H → L + 3, H − 1 → L + 2
	d	11	431	8.13×10^{-2}	*H − 2* → *L*
	e	12	431	8.09×10^{-2}	*H − 2* → *L + 1*
3	a	8	503	7.32×10^{-2}	H → *L* + *2*, H − 1 → L + 1
	b	9	498	5.93×10^{-2}	H − 1 → *L* + *4*
	c	10	482	8.38×10^{-2}	H → *L* + *4*, H − 1 → *L* + *3*, *H − 2* → *L*
	d	13	437	1.32×10^{-1}	*H − 2* → *L* + *2*
	e	14	435	1.65×10^{-1}	*H − 2* → *L* + *3*
	f	15	430	7.10×10^{-2}	*H − 2* → *L* + *4*

[a]The labeled excitations are given in Figs. 5(a) and 5(b).
[b]H − X and L + Y represent HOMO − X and LUMO + Y, respectively.
[c]MOs with z-components are given in italic.

IV. CONCLUSIONS

We synthesized and characterized two novel Au_{13} clusters protected by C2- and C3-bridged diarsine ligands (**2** and **3**). Both clusters had the formula of $[Au_{13}L_5Cl_2]^{3+}$, but their optical properties were markedly different. Successful structure determination of the Au_{13} cluster protected by the C3-bridged diarsines (**3**) allowed us to investigate the effect of bidentate ligands on the geometric and electronic structures of the Au_{13} clusters in comparison with the previously reported Au_{13} cluster bearing C2-bridged diphosphines (**1**). The detailed structure analyses revealed that the methylene bridge of the bidentate ligands is an important factor to cause a slight change in the icosahedral Au_{13} core geometries. From the electronic structure analyses using theoretical calculations, the difference in the Au_{13} core geometries, rather than the coordination atoms (i.e., As or P), was shown to influence the visible absorption profile of the Au_{13} clusters. These results demonstrated that the subtle deformation of the Au_{13} core caused a substantial perturbation of the electronic

structure. In this relation, the experimental absorption spectral pattern of the Au_{13} cluster with C2-bridged arsine (**2**) was unsimilar to either of the spectra of crystallographically defined **1** and **3**, suggesting the presence of another geometry of Au_{13} core. Crystal structure determination of **2** and construction of a unified view to understand the relationship between the geometry and electronic structure of coordinated Au_{13} clusters are worthy of further investigations.

SUPPLEMENTARY MATERIAL

See the supplementary material for crystallographic data for **3** and theoretical data of **1** and **3**.

ACKNOWLEDGMENTS

This work was partly supported by JSPS KAKENHI, Grant Nos. JP17H05345 (Coordination Asymmetry), JP19H02532, and JP18H01987, and the Photoexcitonix Project at Hokkaido University. We thank Professor H. Ito, Dr. T. Seki, and Dr. K. Kato of Hokkaido University for x-ray structural analysis of **3** with the XtaLAB Synergy-DW diffractometer. We also thank Dr. H. Sato of Rigaku Corporation for the help in the crystal data refinement. We are grateful to Professor M. Kato of Hokkaido University for allowing access to the FP-8600 photoluminescence spectrometer.

DATA AVAILABILITY

The data that support the findings of this study are available within the article and its supplementary material. Crystal data of **3** are available in the Cambridge Crystallographic Data Centre at https://www.ccdc.cam.ac.uk, CCDC number: 2082256.

REFERENCES

[1] R. Jin, C. Zeng, M. Zhou, and Y. Chen, Chem. Rev. **116**, 10346 (2016).
[2] K. Konishi, M. Iwasaki, and Y. Shichibu, Acc. Chem. Res. **51**, 3125 (2018).
[3] C. E. Briant, B. R. C. Theobald, J. W. White, L. K. Bell, and D. M. P. Mingos, J. Chem. Soc., Chem. Commun. **1981**, 201.
[4] Y. Shichibu, Y. Negishi, T. Watanabe, N. K. Chaki, H. Kawaguchi, and T. Tsukuda, J. Phys. Chem. C **111**, 7845 (2007).
[5] M. W. Heaven, A. Dass, P. S. White, K. M. Holt, and R. W. Murray, J. Am. Chem. Soc. **130**, 3754 (2008).
[6] Y. Shichibu and K. Konishi, Small **6**, 1216 (2010).
[7] H. Qian, W. T. Eckenhoff, Y. Zhu, T. Pintauer, and R. Jin, J. Am. Chem. Soc. **132**, 8280 (2010).
[8] X.-K. Wan, S.-F. Yuan, Z.-W. Lin, and Q.-M. Wang, Angew. Chem., Int. Ed. **53**, 2923 (2014).
[9] X.-K. Wan, Q. Tang, S.-F. Yuan, D.-e. Jiang, and Q.-M. Wang, J. Am. Chem. Soc. **137**, 652 (2015).
[10] Y. Song, F. Fu, J. Zhang, J. Chai, X. Kang, P. Li, S. Li, H. Zhou, and M. Zhu, Angew. Chem., Int. Ed. **54**, 8430 (2015).
[11] Y. Chen, C. Zeng, C. Liu, K. Kirschbaum, C. Gayathri, R. R. Gil, N. L. Rosi, and R. Jin, J. Am. Chem. Soc. **137**, 10076 (2015).
[12] C. Zeng, Y. Chen, K. Kirschbaum, K. Appavoo, M. Y. Sfeir, and R. Jin, Sci. Adv. **1**, e1500045 (2015).
[13] K. L. D. M. Weerawardene, P. Pandeya, M. Zhou, Y. Chen, R. Jin, and C. M. Aikens, J. Am. Chem. Soc. **141**, 18715 (2019).
[14] H. Hirai, S. Takano, T. Nakamura, and T. Tsukuda, Inorg. Chem. **59**, 17889 (2020).
[15] Y. Shichibu, K. Suzuki, and K. Konishi, Nanoscale **4**, 4125 (2012).
[16] Y.-Z. Li, R. Ganguly, K. Y. Hong, Y. Li, M. E. Tessensohn, R. Webster, and W. K. Leong, Chem. Sci. **9**, 8723 (2018).
[17] M. R. Narouz, S. Takano, P. A. Lummis, T. I. Levchenko, A. Nazemi, S. Kaappa, S. Malola, G. Yousefalizadeh, L. A. Calhoun, K. G. Stamplecoskie, H. Häkkinen, T. Tsukuda, and C. M. Crudden, J. Am. Chem. Soc. **141**, 14997 (2019).
[18] M. Sugiuchi, Y. Shichibu, T. Nakanishi, Y. Hasegawa, and K. Konishi, Chem. Commun. **51**, 13519 (2015).
[19] Z.-H. Gao, J. Dong, Q.-F. Zhang, and L.-S. Wang, Nanoscale Adv. **2**, 4902 (2020).
[20] J. Zhang, Y. Zhou, K. Zheng, H. Abroshan, D. R. Kauffman, J. Sun, and G. Li, Nano Res. **11**, 5787 (2018).
[21] Y. Yang, Q. Zhang, Z.-J. Guan, Z.-A. Nan, J.-Q. Wang, T. Jia, and W.-W. Zhan, Inorg. Chem. **58**, 3670 (2019).
[22] Y. Shichibu, Y. Ogawa, M. Sugiuchi, and K. Konishi, Nanoscale Adv. **3**, 1005 (2021).
[23] R. A. Baber, S. Collard, M. Hooper, A. G. Orpen, P. G. Pringle, M. J. Wilkinson, and R. L. Wingad, Dalton Trans. **2005**, 1491.
[24] J. Carreras, A. Pereira, M. Zanini, and A. M. Echavarren, Organometallics **37**, 3588 (2018).
[25] R. Kobayashi, T. Fujii, H. Imoto, and K. Naka, Eur. J. Inorg. Chem. **2021**, 217.
[26] M. Richter and J. Strähle, Z. Anorg. Allg. Chem. **627**, 918 (2001).
[27] P. Sevillano, O. Fuhr, M. Kattannek, P. Nava, O. Hampe, S. Lebedkin, R. Ahlrichs, D. Fenske, and M. M. Kappes, Angew. Chem., Int. Ed. **45**, 3702 (2006).
[28] S. Tanaka, H. Imoto, T. Kato, and K. Naka, Dalton Trans. **45**, 7937 (2016).
[29] H. Imoto, M. Konishi, S. Nishiyama, H. Sasaki, S. Tanaka, T. Yumura, and K. Naka, Chem. Lett. **48**, 1312 (2019).
[30] M.-C. Brandys, M. C. Jennings, and R. J. Puddephatt, J. Chem. Soc., Dalton Trans. **2000**, 4601.
[31] G. M. Sheldrick, SHELXL-2018, a program for crystal structure refinement, University of Göttingen, 2018.
[32] TURBOMOLE V7.5, 2020.
[33] A. Schäfer, H. Horn, and R. Ahlrichs, J. Chem. Phys. **97**, 2571 (1992).
[34] C. Lee, W. Yang, and R. G. Parr, Phys. Rev. B **37**, 785 (1988).
[35] A. D. Becke, J. Chem. Phys. **98**, 5648 (1993).
[36] F. Weigend and R. Ahlrichs, Phys. Chem. Chem. Phys. **7**, 3297 (2005).
[37] D. Andrae, U. Häußermann, M. Dolg, H. Stoll, and H. Preuß, Theor. Chim. Acta **77**, 123 (1990).
[38] R. Ahlrichs, M. Bär, M. Häser, H. Horn, and C. Kölmel, Chem. Phys. Lett. **162**, 165 (1989).
[39] Y. Li, H. Cheng, T. Yao, Z. Sun, W. Yan, Y. Jiang, Y. Xie, Y. Sun, Y. Huang, S. Liu, J. Zhang, Y. Xie, T. Hu, L. Yang, Z. Wu, and S. Wei, J. Am. Chem. Soc. **134**, 17997 (2012).